Sliding properties of Transition Metal Dichalcogenide bilayers

Pier Luigi Silvestrelli, ¹ S. Subashchandrabose, ² Alberto Ambrosetti, ¹ and Maria Clelia Righi ³ Dipartimento di Fisica e Astronomia, Università degli Studi di Padova, 35131 Padova, Italy

²⁾Centre for Global Health Research, Saveetha Medical College & Hospital, Saveetha Institute of Medical and Technical Sciences (SIMATS), Chennai-602105, India

³⁾Department of Physics and Astronomy, University of Bologna, 40126 Bologna, Italy

(*pierluigi.silvestrelli@unipd.it)

Transition-metal dichalcogenides (TMDs) are valuable as solid lubricants because of their layered structure, which allows for easy shearing along the basal planes. Using Density Functional Theory (DFT) we conducted a first-principles study of the sliding properties of several TMD bilayers: MoS₂, MoTe₂, WS₂, WSe₂, VSe₂, VSe₂, TaSe₂, TaSe₂, TiSe₂, TiSe2, HfS2, ZrS2, MoS2WS2, MoS2VS2. Given the crucial role of van der Waals (vdW) interactions in accurately describing the interlayer interactions in TMD bilayers, we employed vdW-corrected DFT functionals. Our research confirms the dominance of vdW effects by estimating the fraction of interlayer binding energy attributable to these interactions. We also examined how the choice of different vdW-corrected DFT functionals might influence quantitative results. Using MoS₂ as a reference TMD bilayer system, we found that most other TMD bilayers studied exhibit stronger interlayer bonds and greater corrugation. However, TiSe₂ shows a profile similar to MoS₂, while, interestingly, TiS₂, VS₂, and ZrS₂ are characterized by weaker bonding and lower corrugation than MoS₂. We explored relationships between various properties of TMD bilayers, with a particular focus on potential connections between tribological and electronic properties often characteristic of solid interfaces. To this end, we evaluated adhesion energies, work of separation, charge density redistributions in interface regions, differential charge densities, and corrugation. While corrugation and thus resistance to sliding generally tends to increase with the size of the chalcogen element and is typically proportional to the adhesion energy, the relationships between other structural, energetic, and electronic properties do not follow a single, well-defined trend.

I. INTRODUCTION

Transition metal dichalcogenides (TMDs) are twodimensional systems with unique properties that make them central to the current research in solid-state science.¹ In TMDs, a transition metal atom (M) layer is sandwiched between two chalcogen atom (X) layers, and it is commonly assumed that the MX₂ slabs are stacked by van der Waals (vdW) interactions, whereas the intralayer M-X interactions are covalent. The relatively weak, interlayer vdW interactions play a key role in the formation, intercalation, exfoliation and layer-by-layer building of TMD materials, as well as being decisive for their characteristic sliding properties.

The mechanisms underlying the low friction exhibited by TMD materials have been investigated both by first-principles calculations^{2–10} and classical molecular dynamics simulations. ^{11,12} These studies focused on MoS₂ because of its excellent performance for application in devices. Herein we extend the study to the sliding properties of several TMD bilayers: MoS₂, MoTe₂, WSe₂, WSe₂, VSe₂, TaSe₂, TaSe₂, TiSe₂, HfS₂, ZrS₂, MoS₂WS₂, MoS₂VS₂. Our research confirms the dominance of vdW effects by estimating the fraction of the interlayer binding energy attributable to these interactions. We also examined how the choice of different vdW-corrected DFT functionals might influence quantitative results. Using MoS₂ as a reference TMD bilayer system, we found that most other TMD bilayers studied exhibit

stronger interlayer bonds and greater corrugation. However, TiSe₂ shows a profile similar to MoS₂, while TiS₂, VS₂, and ZrS₂ are characterized by weaker bonding and less corrugation than MoS₂. We explored relationships between various properties of TMD bilayers, with a particular focus on potential connections between tribological and electronic properties often characteristic of solid interfaces. To this end, we evaluated interlayer binding energies (also known as adhesion energies), charge density redistributions in interface regions, differential charge densities, and corrugation.

II. METHOD

Our first principles study was performed using the Quantum ESPRESSO (QE) package, ^{13,14} based on the DFT. ^{15–17} In most of the calculations the PBE ¹⁸ exchange-correlation functional was employed, combined with the semiempirical Grimme correction ¹⁹ to properly describe vdW interactions, as done in previous studies on TMDs; ^{20,21} hereafter we refer to this functional as DFT-D2. However, other vdW-corrected DFT functionals have been also used (see Results section) to assess the effect of alternative schemes. Clearly, the importance of vdW interactions in the characterization of layered TMD systems and more generally in materials cannot be overemphasized (see, for istance, refs. 22 and 23).

Wavefunctions were expanded in plane waves with a ki-

netic energy cutoff in the range 50-55 Ry, depending on the constituents atoms. A $12 \times 12 \times 12$ and a $12 \times 12 \times 1$ k-point Monkhorst-Pack grid was used to sample the Brillouin Zone for TMD bulk and bilayer structures, respectively. In all systems an hexagonal cell was used, containing a MX₂ unit per layer (M=transition metal atom, X=chalcogen atom). When monolayers or bilayers were modeled, the c dimension of the cell was enlarged so to allow at least 12 Å of vacuum between replicated images: the number of k points along such direction was consequently reduced to one.

The interlayer binding energy E_b is obtained as

$$E_b = E_{12} - E_1 - E_2 \tag{1}$$

where E_{12} is the energy of the optimized bilayer and E_1 and E_2 the energies of the single optimized layers. The work of separation $W_{\rm sep}$, defined as the energy per unit area required to separate two layers from equilibrium to infinite distance, is calculated as $W_{\rm sep} = |E_b|/A$, where A is the unit-cell area. $W_{\rm sep}$ can therefore be properly compared among systems having different cell sizes. The maximum sliding corrugation is indicated as $W_{\rm max}$.

III. RESULTS AND DISCUSSIONS

Here we present the results of our first-principles study (mainly based on the DFT-D2 functional¹⁹) of selected TMD bilayers, namely: MoS₂, MoTe₂, WSe₂, WSe₂, VSe₂, VSe₂, TaSe₂, TaSe₂, TiSe₂, HfS₂, ZrS₂, MoS₂WS₂, MoS₂VS₂.

The most common configurations assumed by the TMDs are the 1T-trigonal and 2H-octahedral ones (see Fig. 1). 1Ttrigonal is characterized by a trigonal symmetry with a single layer of transition metal atoms arranged between two layers of chalcogen atoms in an octahedral geometry, while 2Hoctahedral is characterized by an hexagonal symmetry with two layers of transition metal atoms arranged between layers of chalcogen atoms in a trigonal prismatic geometry. The latter configuration is generally more stable and common for many TMDs, including (within our list) MoS₂, WS₂, WSe₂, MoTe₂; instead 1T-trigonal is metastable for many TMDs but it is favored in a few cases, such as TiS2, TaS2, TaSe2, and HfS₂. VS₂ and VSe₂ are reported to prefer the 1T-trigonal form but can also exist in the 2*H-octahedral* one under certain conditions. These preferences are mainly due to the electronic configuration of the transition metal atoms and their interactions with the chalcogen atoms. Differently from, for instance, graphene, where two commensurate planes always show the same relative orientation, TMDs have an additional degree of freedom when forming the bilayer: in fact the layers can be either parallel or antiparallel. Here we have investigated both orientations, labeled R0 and R180, respectively.^{20,21} In fact, while most investigations on TMDs have dealt with the R180 structure (typical of the 2H polytype), examples of 3R polytypes presenting the R0 orientation were found in both natural and synthetic crystals.^{24,25} A previous study²⁰ showed that for MoS₂ R0 and R180 bilayers are degenerate at zero applied load while the degeneracy is instead removed by uniaxial stress.

TABLE I. Calculated values for the lattice constant a, interlayer distance d_{int} , work of separation W_{sep} , and maximum sliding corrugation W_{max} for TMD bilayers in 2H-octahedral configuration. Distances are in Å and energies in J/m^2 ; R0 or R180 denote parallel or antiparallel orientation of bilayers. Where available, experimental (from refs. 26) and RPA reference values (from ref. 24) are reported in parentheses for comparison.

system	а	$d_{ m int}$	W_{sep}	$W_{\rm max}$
MoS ₂ R0	3.198	6.208	0.277	0.100
MoS ₂ R180	3.198	6.218	0.277	0.096
	(3.160)	(6.27)	(0.300)	(0.127)
MoTe ₂ R0	3.524	7.036	0.484	0.202
MoTe ₂ R180	3.524	7.031	0.505	0.215
WS ₂ R0	3.180	6.006	0.497	0.167
WS ₂ R180	3.180	6.179	0.497	0.161
	(3.153)	(6.24)	(0.308)	(0.141)
WSe ₂ R0	3.327	6.402	0.569	0.200
WSe ₂ R180	3.327	6.466	0.575	0.198
	(3.282)	(6.50)	(0.308)	(0.136)
VS ₂ R0	3.175	6.045	0.247	0.091
VS ₂ R180	3.175	6.078	0.252	0.095
VSe ₂ R0	3.328	6.383	0.327	0.120
VSe ₂ R180	3.328	6.410	0.324	0.114
TaS ₂ R0	3.345	6.002	0.486	0.151
TaS ₂ R180	3.345	5.915	0.503	0.167
TaSe ₂ R0	3.477	6.330	0.529	0.185
TaSe ₂ R180	3.477	6.256	0.542	0.198
TiS ₂ R0	3.329	6.145	0.201	0.065
TiS ₂ R180	3.329	5.954	0.177	0.091

TABLE II. Calculated values for the lattice constant a, interlayer distance $d_{\rm int}$, work of separation $W_{\rm sep}$, and maximum sliding corrugation $W_{\rm max}$ for TMD bilayers in *1T-trigonal* configuration. Distances are in Å and energies in J/m²; R0 or R180 denote parallel or antiparallel orientation of bilayers.

system	a	$d_{ m int}$	$W_{\rm sep}$	$W_{\rm max}$
MoS ₂ R0	3.227	6.009	0.316	0.123
MoS ₂ R180	3.227	5.990	0.334	0.142
VS ₂ R0	3.193	5.947	0.258	0.093
VS ₂ R180	3.193	5.994	0.250	0.088
VSe ₂ R0	3.344	6.288	0.341	0.123
VSe ₂ R180	3.344	6.319	0.340	0.125
TaS ₂ R0	3.393	5.803	0.466	0.159
TaS ₂ R180	3.393	5.886	0.455	0.151
TaSe ₂ R0	3.509	6.174	0.550	0.193
TaSe ₂ R180	3.509	6.250	0.534	0.179
TiS ₂ R0	3.392	5.852	0.218	0.078
TiS ₂ R180	3.392	5.952	0.196	0.055
TiSe ₂ R0	3.510	6.188	0.315	0.120
TiSe ₂ R180	3.510	6.277	0.288	0.091
HfS ₂ R0	3.623	5.679	0.421	0.147
HfS ₂ R180	3.623	5.729	0.401	0.126
ZrS ₂ R0	3.632	5.935	0.200	0.069
ZrS ₂ R180	3.632	6.005	0.185	0.053

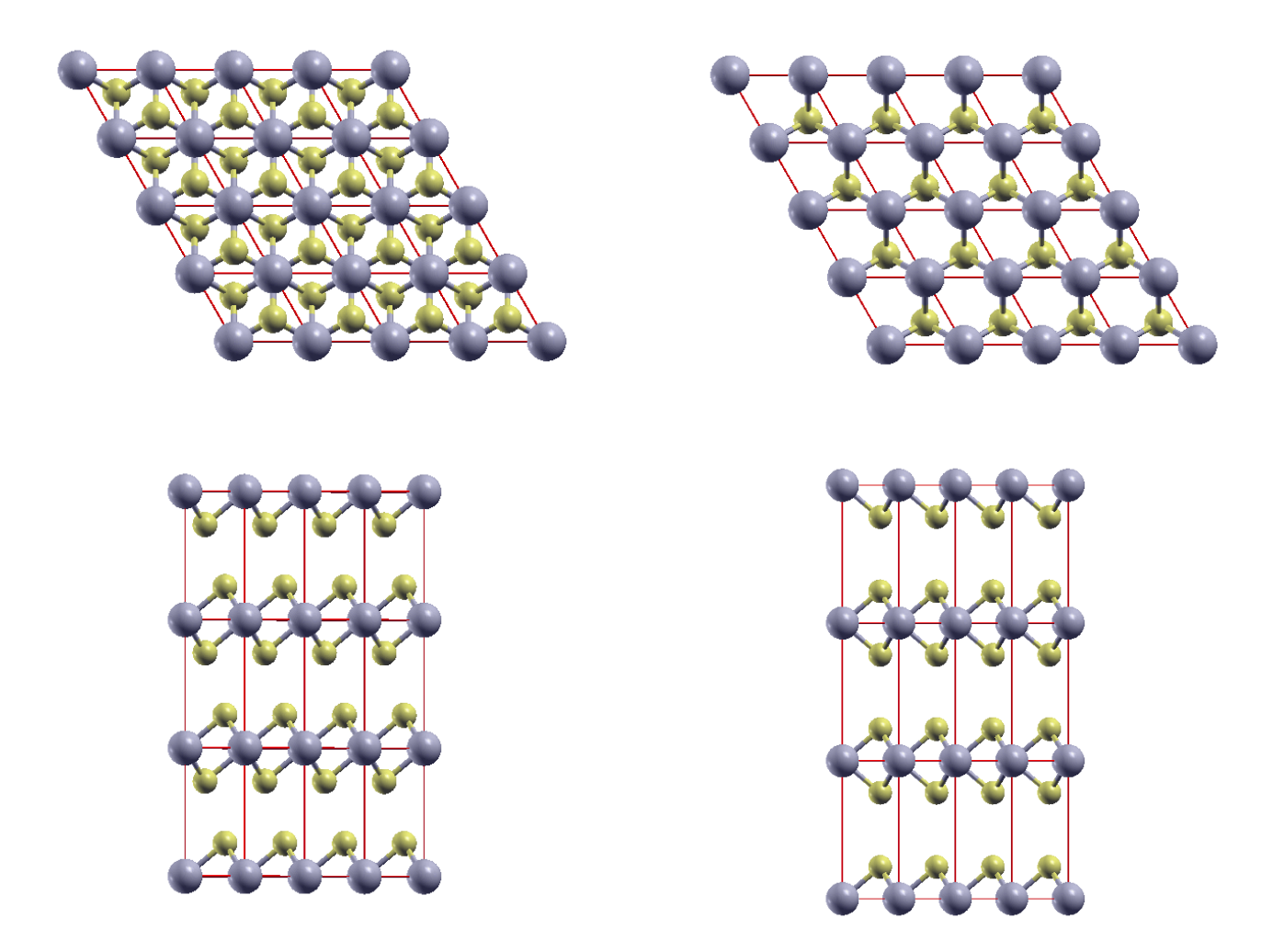


FIG. 1(a). Bulk MoS₂ in *1T-trigonal* configuration. Upper figure: top view; lower figure: side view. The unit cells are marked with red solid lines; Mo atoms are represented in gray and S atoms in yellow.

FIG. 1(b). Bulk MoS_2 in 2H-octahedral configuration. Upper figure: top view; lower figure: side view. The unit cells are marked with red solid lines; Mo atoms are represented in gray and S atoms in yellow.

Tables I and II report the value of the lattice constant *a* and of the optimized interlayer distance *d*_{int} (between transition metal atoms M in different layers). *a* has been determined by optimizing the cell parameters of the TMD systems by considering their bulk structure. Note that, while our calculations confirm that for bulk MoS₂ the *2H-octahedral* structure is energetically favored over the *1T-trigonal* one (by about 0.7 eV per unit cell), in the case of MoS₂ bilayer the opposite is found (see Tables I and II). For most of the investigated TMD bilayers we have considered both the *1T-trigonal* and *2H-octahedral* configurations since the binding energies of both the structures are comparable.

As can be seen in Tables I and II, compounds containing sulfur (S) tend to have lower *a* values compared to their selenium (Se) or tellurium (Te) analogs, while compounds with heavier metals than Mo, such as W, Ta, and Hf, tend to have higher *a* values. A general, approximate positive correlation

exists between a and $d_{\rm int}$: compounds with larger a tend to have larger interlayer distance. Moreover, a, $d_{\rm int}$, and $W_{\rm sep}$ values increase, for the same M element, going from S to Se and to Te: in fact a larger polarizability of the interfacial chalcogen atoms leads to stronger vdW interactions between the layers, in line with previous findings. Considering the lowest-energy configuration, WSe₂ has the highest $W_{\rm sep}$ value, followed by TaSe₂ and MoTe₂, while ZrS₂ and TiS₂ have the lowest values. Clearly these correlations can be explained by considering the atomic sizes, electronegativity, and electronic structure of the various elements involved.

Interestingly, there is a strong positive correlation between W_{sep} and the maximum sliding corrugation W_{max} : TMD bilayers with higher W_{sep} values tend to have higher corrugations: $W_{\text{max}} \sim 0.35 W_{\text{sep}}$, which agrees with the general understanding that stronger interlayer bonding leads to higher corrugation and friction. Note that a similar correlation was also

found²⁷ for metal interfaces (the cleavage strength is directly proportional to the adhesion); moreover an expression for the corrugation related to the repulsive part of the intralayer adhesion was suggested²⁸ for the graphene bilayer. Moderate deviations from this trend are represented by VSe₂ (smaller corrugation than expected) and MoTe₂ (larger corrugation than expected). Tables I and II therefore exhibit several notable correlations among the reported TMD properties, with W_{sep} appearing to be a central parameter that correlates well with both interlayer distance and energy corrugation values, as also observed in previous DFT studies.²⁹ The choice of metal and chalcogen atoms significantly influences these properties as well, with heavier elements generally leading to stronger interlayer interactions and more corrugated energy landscapes. Larger interfacial atoms on the one hand increase the adhesion, due to the stronger van der Waals interlayer forces; on the other, they increase the corrugation, due to the Pauli repulsion between electronic clouds of on-top chalcogen-chalcogen structures (corresponding to the potential-energy maxima). It was shown that vdW interactions do not contribute significantly to the corrugation;²⁸ in the case of graphene, in fact, a much lower corrugation with respect to MoS₂ is observed, despite their almost equal adhesion energies. For almost all systems considered, the corrugation $W_{\rm max}$ is larger than in the case of graphene where $W_{\text{max}} = 0.060 \text{ J/m}^2$; 21 notable exceptions are represented by TiS₂ and ZrS₂ bilayers in the 1T-trigonal configuration with R180 orientation, which are characterized by a corrugation even slightly lower than that of graphene (see Table II).

Note that VS₂ and VSe₂ have ferromagnetic properties, as confirmed by our DFT calculations: in fact for VS2 we find a total magnetic moment of about 1.1 and 1.8 Bohr magneton per unit cell in the 1T-trigonal and 2H-octahedral configuration, respectively, while, for VSe2, the corresponding values are 1.3 and 1.9 Bohr magneton per unit cell. Actually these systems are classified as "strongly correlated materials", with VSe₂ which is attractive for van der Waals spintronics applications $^{30-32}$ and VS₂ which is not very stable; 32,33 there are several factors contributing to VS2 instability: in particular, VS₂ monolayers tend to undergo a structural distortion (structural and dyamical instability); moreover partially filled d-orbitals of vanadium make it prone to electronic instabilities leading to magnetic ordering, and make VS₂ monolayers chemically very active. Calculations were performed for these system also using a more suitable Hubbard LDA+U approach (with U=1.0 eV);³⁴ however no significant changes were found with respect to the standard method. For instance, in the case of the 2H-octahedral R0 configuration of VS₂, $W_{\rm max}$ is slightly smaller with Hubbard LDA+U, the reduction being of about 9%.

In Figs. 2 and 3 we plot the variation of the interlayer binding energy per unit-cell area E_b/A in our TMD bilayers. Each profile is associated with the sliding of the bilayer, along a specified path, as exemplified by the y direction indicated by the blue arrow in Fig. 4. Symbols correspond to calculated data; lines are just guides for the eyes. Since the R180 structure appears to be preferred by most of systems in the 2H-octahedral configuration (which is typical of the 2H

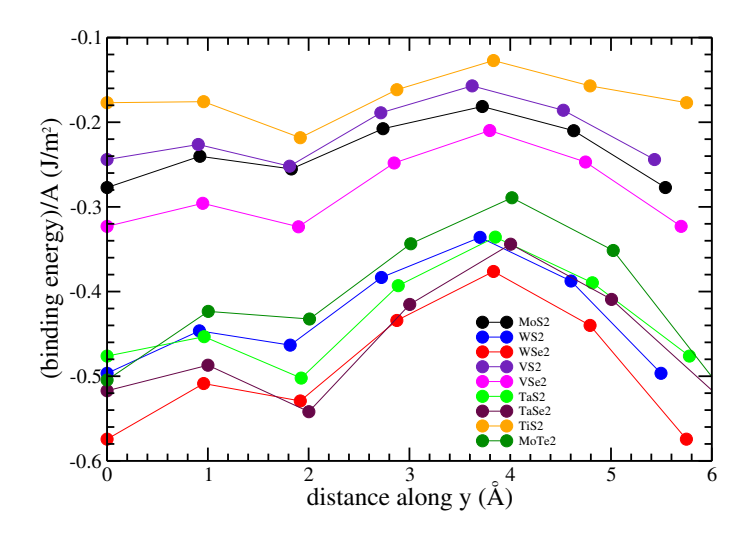


FIG. 2. Variation of the interlayer binding energy per unit-cell area, E_b/A , in different TMD bilayers, considering the R180 structure for 2H-octahedral configurations. Each profile is associated with the sliding of the bilayer, along the path in the y direction indicated by the blue arrow in Fig. 4. Symbols correspond to calculated data; lines are just guides for the eyes.

polytype²¹), while the R0 structure is instead favored by most of the systems in the *1T-trigonal* configuration, we only plot data relative to the R180 structure for *2H-octahedral* configurations (Fig. 2) and data relative to the R0 structure for *1T-trigonal* configurations (Fig. 3). In any case, for a given system, Tables I and II show that the energy differences between R0 and R180 structures are at most moderate; for instance, we find that in the case of MoS₂ R0 and R180 bilayers are essentially degenerate, in line with previous reports at zero load.²¹ More significant differences between R0 and R180 structures are instead expected in simulations with an applied load.²¹

Obviously, the more negative the values, the stronger the interaction between the two layers. As can be seen, Figs. 2 and 3 show that (see also Tables I and II) with respect to the MoS₂ case, taken as a reference, almost all the other bilayers are characterized by stronger interlayer bonds and greater corrugation, but for the TiSe2 system which exhibits a profile similar to that of MoS₂, and for TiS₂, VS₂, and ZrS₂ bilayers which appear less bonded and less corrugated than MoS₂. Interestingly, the TMD bilayers which are less corrugated than MoS₂ (TiS₂, VS₂, ZrS₂) are all characterized by a difference between the Pauling electronegativity of the chalcogen and the metal element that is larger than in MoS₂, thus partially supporting the conjecture of Irving et al.²⁹ who proposed that intrinsic frictional properties of TMD compounds can be effectively guessed from a property as simple as atomic electronegativity: slippage between planes should be facilitated by the presence of enhanced (slightly decreased) charge accumulation on the chalcogens (metals). However, our results suggest that this conclusion is not valid in general, as demonstrated

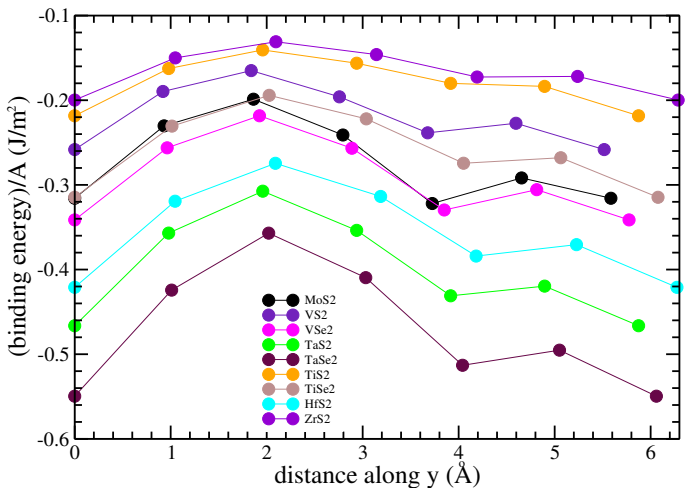


FIG. 3. Variation of the interlayer binding energy per unit-cell area, E_b/A , in different TMD bilayers, considering the R0 structure for *1T-trigonal* configurations. Each profile is associated with the sliding of the bilayer, along the path in the y direction indicated by the blue arrow in Fig. 4. Symbols correspond to calculated data; lines are just guides for the eyes.

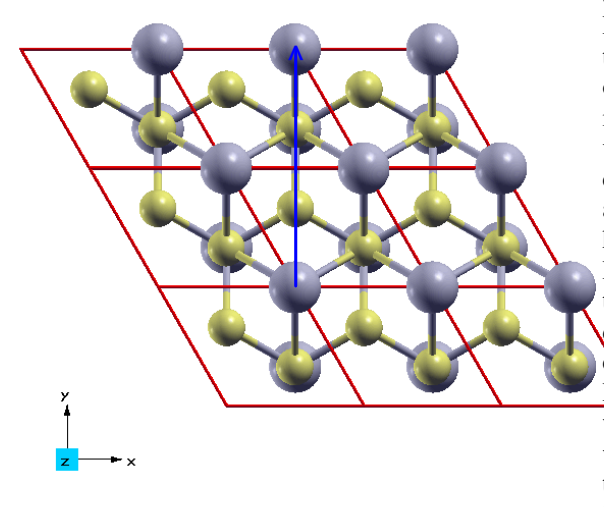


FIG. 4. Sliding path (indicated by the blue arrow) relative to the R0 structure in the 2H-octahedral configuration of MoS_2 (top view). The unit cells are marked with red solid lines; Mo atoms are represented in gray and S atoms in yellow.

by the fact that several TMD bilayers (HfS₂, TaS₂, TaSe₂, TiSe₂, VSe₂) exhibit higher (or at most similar) corrugation than MoS₂, despite a larger difference between the electronegativity of the chalcogen and the metal element. In line with previous DFT studies,²⁹ we find that larger chalco-

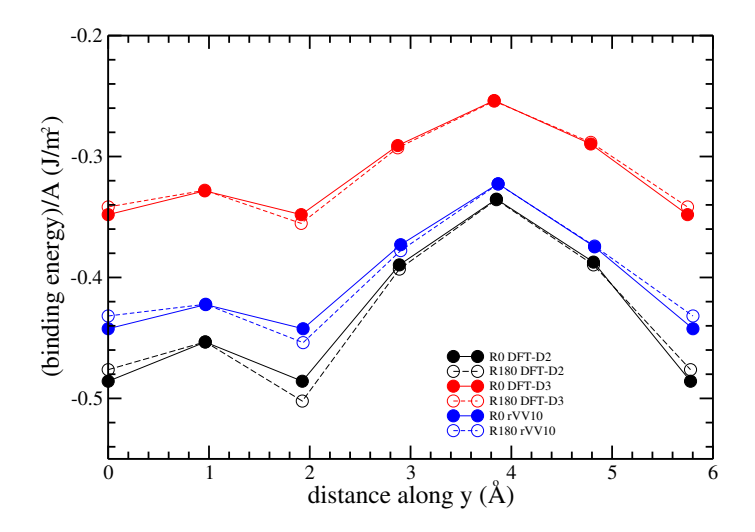
TABLE III. Calculated values for the lattice constant a, interlayer distance $d_{\rm int}$, work of separation $W_{\rm sep}$, and maximum sliding corrugation $W_{\rm max}$ considering the 2H-octahedral configuration of TaS $_2$ with R0 or R180 orientation of bilayers, using different vdW-corrected DFT functionals. Distances are in Å and energies in J/m 2 .

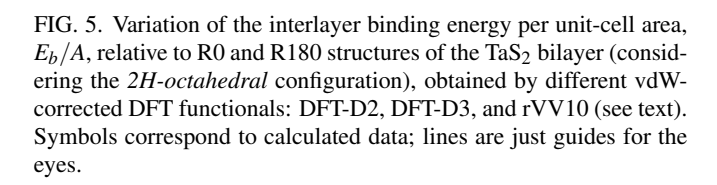
DFT functional	а	d_{int}	$W_{\rm sep}$	$W_{\rm max}$
		6.002		
DFT-D2 R180	3.345	5.915	0.503	0.167
	3.319			
DFT-D3 R180	3.319	6.193	0.355	0.101
	3.351			
rVV10 R180	3.351	6.194	0.454	0.131

gen atoms lead to stronger interlayer binding. Also note that, in the case of the R180 structure for *2H-octahedral* configurations, while in most systems we considered, the starting position coincides with the lowest-energy minimum (characterized by the chalcogen atoms in the top layer sitting directly above the metal atoms in the bottom layer^{21,29}), in the case of TaS₂, TaSe₂, VS₂, and VSe₂ the structure corresponding to a displaced position is instead energetically favored.

In order to assess to what extent our reported quantitative results can depend on the choice of the adopted DFT functional, in Fig. 5 and Table III we compare, in the selected case of the TaS₂ TMD bilayer (considering the 2H-octahedral configuration), the energy profiles obtained by DFT-D2 to those obtained by other vdW-corrected DFT functionals: DFT-D3,³⁵ in which the molecular environment of a given atom is taken into account by the empirical concept of fractional coordination number, and the rVV10 functional³⁶ (the revised, more efficient version of the original VV10 scheme³⁷), where vdW effects are included by introducing an explicitly nonlocal correlation functional. As can be seen, the energy profiles of all the three functionals exhibit a similar qualitative behavior; however significant quantitative differences are evident. The DFT-D3 binding energies are quite smaller (in absolute value) than the DFT-D2 ones, while instead rVV10 gives intermediate values between DFT-D3 and DFT-D2, being however loser to those of DFT-D2. By comparing DFT-D3 with DFT-Da from Table III, one can also see that with DFT-D3 the weaker bonding is consistent with larger interlayer distances, while instead, with the rVV10 functional, the interlayer distances are comparable with those of DFT-D3. Similar changes in binding energy, using the three different DFT functionals, were also observed in the TiS₂ bilayer. Therefore the choice of a specific vdW-corrected DFT functional can significantly influence the quantitative results, as already discussed in other theoretical studies on TMDs (see, for instance, ref. 38).

By using the semiempirical DFT-D2 and DFT-D3 functionals, one can also easily estimate the fraction of the interlayer binding energy that can be ascribed to vdW interactions. As expected for this kind of bilayer systems, the vdW interactions are predominant (see Fig. 6, again for the TaS₂ system): quantitatively, at the optimal, equilibrium interlayer distance, the vdW fraction of the binding energy is 98% and 110% with DFT-D2 and DFT-D3, respectively; in the latter case this





means that the energy due to other types of interactions is positive (repulsive contribution).

Interestingly, in ref.39 a connection between the intrinsic tribological properties and the electronic properties of a solid interface was pointed out. In particular, the adhesion and frictional forces seem to be determined by the electronic charge redistribution occurring due to the relative displacements of the two surfaces in contact. To verify to what extent this conclusion is applicable to our investigated systems, the relations between different quantities have been considered for selected TMD bilayers with the R180 structure in the 2H-octahedral configuration. In Figs. S1 and S2 in supplementary material, and in Fig. 7 the work of separation W_{sep} is related to the redistribution of charge density in the interface region (ρ_{redist} , as defined in ref.39), the height h of the central peak of the planar average of the differential density³⁹ and the maximum sliding corrugation W_{max} , respectively. Analysis of these figures indicates that: i) W_{max} turns out to be proportional to W_{sep} (Fig. 7), in line with the general behavior observed above and with the results of ref.39; ii) ρ_{redist} and h are instead proportional to W_{sep} only considering a given M element (for instance Ta in TaS₂ and TaSe₂, and W in WS₂ and WSe₂) and changing the chalcogen element, while the same is not true considering a given chalcogen element (for instance S in MoS₂, WS₂ and TaS₂) and changing the M element; note however the exception represented by the VS₂ and VSe₂ systems, since ρ_{redist} is larger for VS₂ than for VSe₂.

Moreover, Fig. 8 and Fig. S3 (in supplementary material) suggest that both $\rho_{\rm redist}$ and the maximum corrugation $W_{\rm max}$ are proportional to the lattice constant of the system,

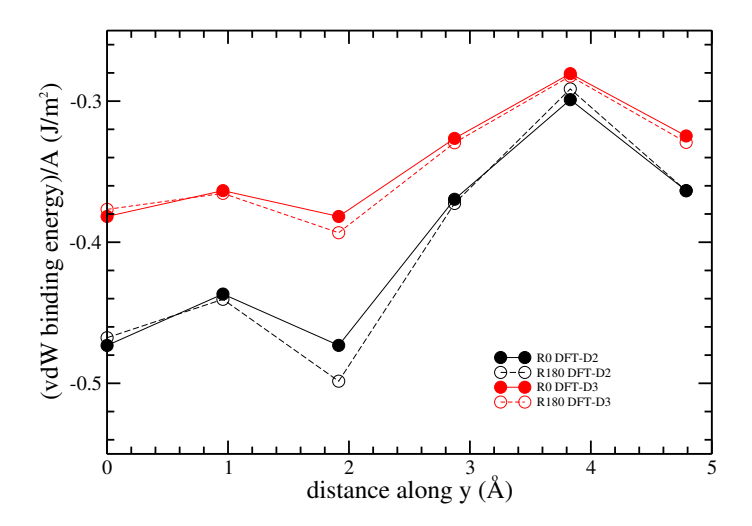


FIG. 6. Variation of the interlayer binding energy per unit-cell area, considering the vdW contribution only, relative to R0 and R180 structures of the TaS_2 bilayer (in the 2H-octahedral configuration), obtained by the DFT-D2 and DFT-D3 functionals. Symbols correspond to calculated data; lines are just guides for the eyes.

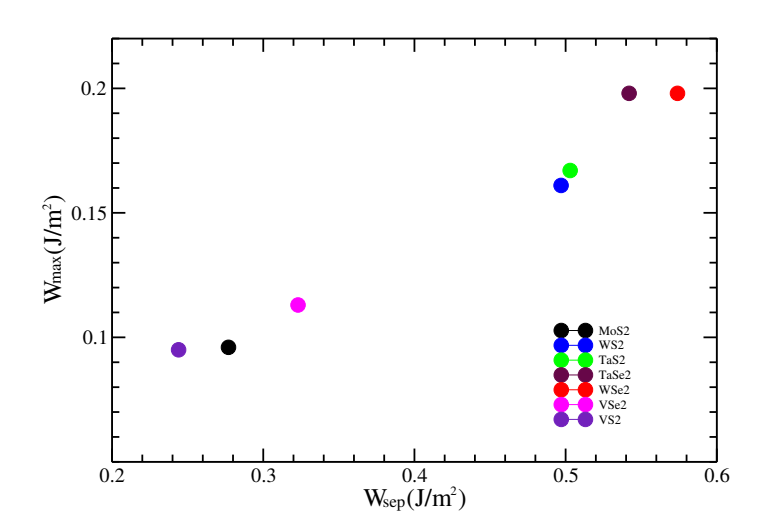


FIG. 7. Maximum sliding corrugation $W_{\rm max}$ versus work of separation $W_{\rm sep}$ for selected TMD bilayers with the R180 structure in the 2H-octahedral configuration.

by changing the chalcogen element, so that friction seems to increase as a function of the size of the chalcogen element (from S to Se), in line with the results of previous DFT calculations, ^{21,29} most likely due to the increased Pauli repulsion. Apparently in ref.40 the opposite effect was found, however it must be pointed out that the nanoscale friction behavior reported in that study was obtained by a different approach,

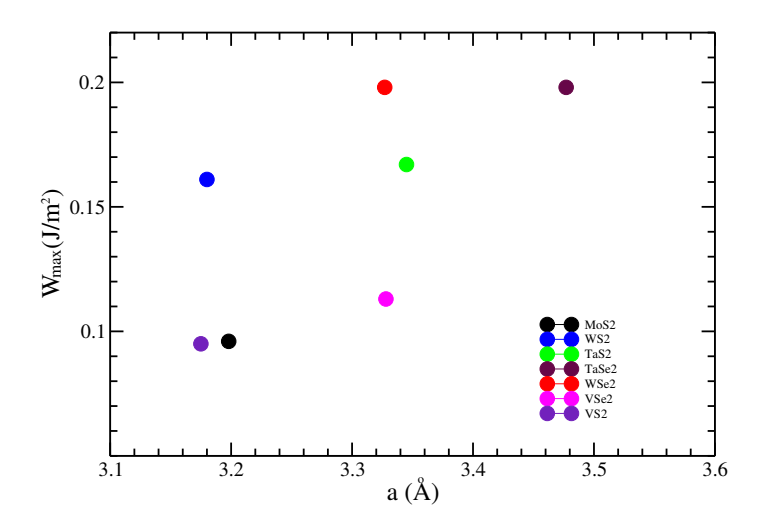


FIG. 8. Maximum sliding corrugation W_{max} versus lattice constant a for selected TMD bilayers with the R180 structure in the 2H-octahedral configuration.

TABLE IV. Calculated values for the lattice constant a, work of separation W_{sep} , and maximum sliding corrugation W_{max} for two bilayers composed of different monolayers (heterostructures) in 2H-octahedral configuration with R0 orientation, compared to data relative to the corresponding bilayers composed of identical monolayers (homostructures). a is in Å and energies in J/m^2 .

system	a	W_{sep}	$W_{\rm max}$
MoS_2WS_2	3.184	0.368	0.129
MoS_2VS_2	3.175	0.199	0.110
MoS ₂	3.198	0.277	0.100
WS_2	3.180	0.497	0.167
VS_2	3.175	0.247	0.091

considering "a tip sliding on a TMD" instead of "sliding between two TMD layers". Note again the peculiar VS_2 and VSe_2 cases: ρ_{redist} is larger in VS_2 than in VSe_2 , in spite of the fact that the lattice constant of VS_2 is smaller. The critical role of the lattice constant in determining the frictional behavior at the nanoscale is in line with previous investigations.⁴⁰

We have also cosidered a pair of *heterostuctures*, namely two bilayers each composed of two different TMD monolayers: MoS_2WS_2 and MoS_2VS_2 . As can be seen in Table IV and Figs. 9 and 10, MoS_2WS_2 is characterized by W_{sep} and W_{max} values intermediate between those of the MoS_2 and WS_2 bilayers, while instead in MoS_2VS_2 W_{sep} and W_{max} are smaller and larger, respectively than those of the MoS_2 and VS_2 bilayers, again showing a peculiar behavior of TMD systems containing the V element.

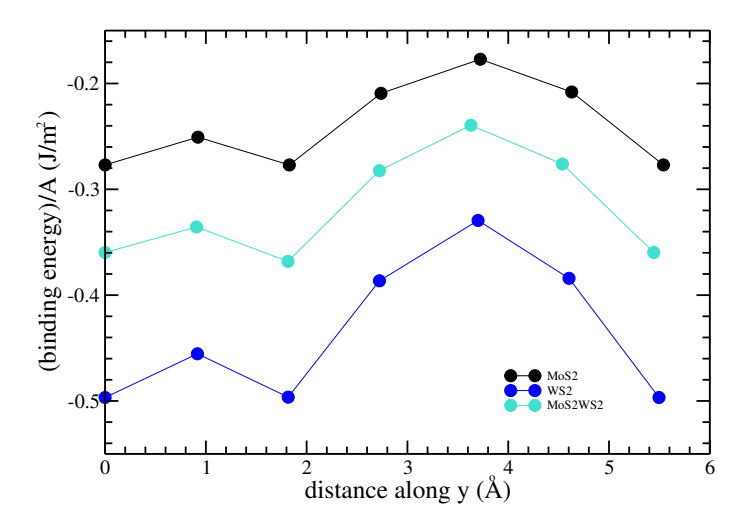


FIG. 9. Variation of the interlayer binding energy per unit-cell area, E_b/A , in MoS₂, WS₂ bilayers, and MoS₂WS₂ heterostructure, considering the R0 orientation and the *2H-octahedral* configuration. Symbols correspond to calculated data; lines are just guides for the eyes.

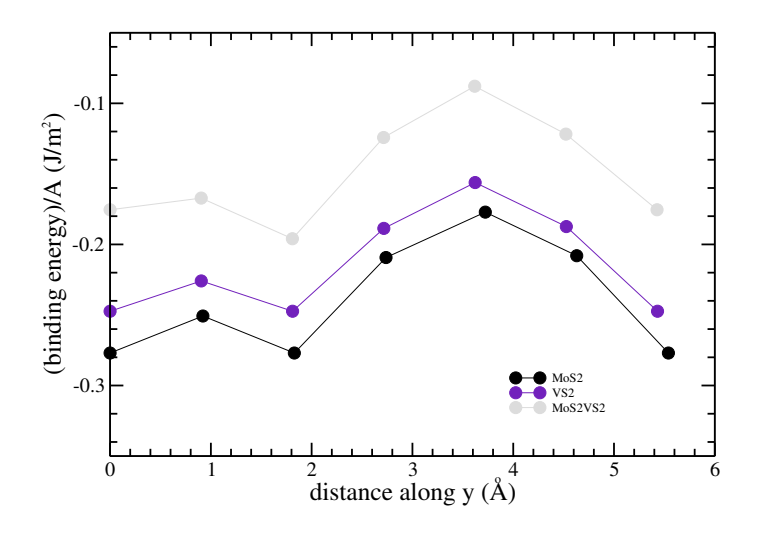


FIG. 10. Variation of the interlayer binding energy per unit-cell area, E_b/A , in MoS₂, VS₂ bilayers, and MoS₂VS₂ heterostructure, considering the R0 orientation and the *2H-octahedral* configuration. Symbols correspond to calculated data; lines are just guides for the eyes.

IV. CONCLUSIONS

We have presented the results of a first principles, DFT investigation, of the energetic and electronic properties of several TMD bilayers by particularly focusing on their sliding

properties. The R180 structure appears to be preferred by most of systems in the 2H-octahedral configuration, while the R0 structure is instead favored by most of the systems in the 1T-trigonal configuration. Our investigation substantiates the prevalence of van der Waals (vdW) interactions by quantifying their contribution to interlayer cohesion. We also assessed the impact of different vdW-corrected Density Functional Theory (DFT) functionals on our numerical outcomes. Using MoS₂ as a benchmark, we observed that most other TMDs exhibit enhanced interlayer bonding and corrugation. Notably, TiSe₂ displays characteristics akin to MoS₂, while TiS₂, VS₂, and ZrS₂ demonstrate reduced bonding strength and corrugation compared to MoS₂, which makes them promising for applications in fields such as nanoelectronics, optoelectronics, and sensing technologies. Interestingly, the corrugation and thus the energy barriers for interlayer sliding generally increases with the size of the chalcogen element; moreover, it is even slightly lower than that of graphene for selected configurations of TiS2 and ZrS2 bilayers. We also investigated correlations among various TMD bilayer properties, with particular emphasis on potential links between tribological and electronic characteristics often associated with solid interfaces, considering adhesion energies, interfacial charge density redistributions, differential charge densities, and corrugation patterns. We found that, while the corrugation is typically proportional to the adhesion energy, the interplay between most structural, energetic, and electronic properties does not adhere to a single, clearly defined pattern. This complexity underscores the multifaceted nature of TMD bilayer systems and highlights the need for comprehensive studies to fully understand their behavior. The observation of a strong positive correlation between W_{sep} and the maximum sliding corrugation $W_{\rm max}$ ($W_{\rm max} \sim 0.35 W_{\rm sep}$) has important implications for further theoretical and experimental investigations aimed at developing a comprehensive understanding of the tribological properties of TMDs: the effect of external factors, such as applied pressure, temperature, or the presence of defects or impurities, on the W_{sep} - W_{max} correlation could be studied to understand their influence on the sliding behavior; the correlation could be investigated under different environmental conditions (for example in the presence humidity); experiments could be designed to study the evolution of the W_{sep} - W_{max} correlation as a function of sliding distance or cycles, which could provide insights into the wear and degradation mechanisms of TMD interfaces.

V. SUPPLEMENTARY MATERIAL

See the supplementary material for further figures illustrating the connection between the intrinsic tribological properties and the electronic properties for selected TMD bilayers with the R180 structure in the 2H-octahedral configuration: the work of separation $W_{\rm sep}$ versus the redistribution of charge density in the interface region $\rho_{\rm redist}$ and versus the height h of the central peak of the planar average of the differential density; the lattice constant a versus $\rho_{\rm redist}$.

VI. ACKNOWLEDGEMENTS

These results are part of the "Advancing Solid Interface and Lubricants by First Principles Material Design (SLIDE)" project that has received funding from the European Research Council (ERC) under the European Union's Horizon 2020 research and innovation program (Grant agreement No. 865633).

- ¹D. L. Duong, S. J. Yun, Y. H. Lee, "van der Waals Layered Materials: Opportunities and Challenges", ACS Nano 11, 11803 (2017).
- ²S. Cahangirov, C. Ataca, M. Topsakal, H. Sahin, and S. Ciraci, "Frictional Figures of Merit for Single Layered Nanostructures", Phys. Rev. Lett. **108**, 126103 (2012).
- ³H. Peelaers and C. G. Van de Walle, "Elastic constants and pressure-induced effects in MoS₂", J. Phys. Chem. C **118**, 12073 (2014).
- ⁴L. Hromadová, R. Martoñák, and E. Tosatti, "Structure change, layer sliding, and metallization in high-pressure MoS₂", Phys. Rev. B 87, 144105 (2013).
- ⁵T. Liang, W. G. Sawyer, S. S. Perry, S. B. Sinnott, and S. R. Phillpot, "First-principles determination of static potential energy surfaces for atomic friction on MoS₂ and MoO₃", Phys. Rev. B **77**, 104105 (2008).
- ⁶A. Blumberg, U. Keshet, I. Zaltsman, and O. Hod, "Interlayer registry to determine the sliding potential of layered metal dichalcogenides: The Case of 2H-MoS₂", J. Phys. Chem. Lett. **3**, 1936 (2012).
- ⁷L. Wang, X. Zhou, T. Ma, D. Liu, L. Gao, X. Li, J. Zhang, Y. Hu, H. Wang, Y. Dai, and J. Luo, "Superlubricity of a graphene/MoS₂ heterostructure: a combined experimental and DFT study", Nanoscale 9, 10846 (2017).
- ⁸G. Levita, P. Restuccia, M. C. Righi, "Graphene and MoS₂ interacting with water: A comparison by ab initio calculations", Carbon 107, 878 (2016).
- ⁹G. Levita, M. C. Righi, "Effects of Water Intercalation and Tribochemistry on MoS₂ Lubricity: An Ab Initio Molecular Dynamics Investigation", ChemPhysChem 18, 1475 (2017).
- ¹⁰M. Stella, C. D. Lorenz, M. C. Righi, "Effects of intercalated water on the lubricity of sliding layers under load: a theoretical investigation on MoS₂", 2D Mater. 8, 035052 (2021).
- ¹¹T. Onodera, Y. Morita, A. Suzuki, M. Koyama, H. Tsuboi, N. Hatakeyama, A. Endou, H. Takaba, M. Kubo, F. Dassenoy, C. Minfray, L. Joly-Pottuz, J.-M. Martin, and A. Miyamoto, "A computational chemistry study on friction of h-MoS₂. Part I. mechanism of single sheet lubrication", J. Phys. Chem. B 113, 16526 (2009).
- ¹²M. Stefanov, A. N. Enyashin, T. Heine, and G. Seifert, "Nanolubrication: How do MoS₂-based nanostructures lubricate?", J. Phys. Chem. C **112**, 17764 (2008)
- ¹³P. Giannozzi, S. Baroni, N. Bonini, M. Calandra, R. Car, C. Cavazzoni, D. Ceresoli, G. L. Chiarotti, M. Cococcioni, I. Dabo, "QUANTUM ESPRESSO: a modular and open-source software project for quantum simulations of materials", Journal of Physics: Condensed Matter 21, 395502 (2009).
- ¹⁴P. Giannozzi, O. Andreussi, T. Brumme, O. Bunau, M. Buongiorno Nardelli, M. Calandra, R. Car, C. Cavazzoni, D. Ceresoli, M. Cococcioni *et al.*, "Advanced capabilities for materials modelling with Quantum ESPRESSO", Journal of Physics: Condensed Matter 29, 465901 (2017).
- ¹⁵P. Hoenberg and W. Kohn, "Inhomogeneus Electron Gas", Phys. Rev. 136, B864 (1964).
- ¹⁶W. Kohn and L. J. Sham, "Self-Consistent Equations Including Exchange and Correlation Effects", Phys. Rev. **140**, A1133 (1965).
- ¹⁷R. Car and M. Parrinello, "Unified Approach for MD and DFT", Phys. Rev. Lett. **55**, 2471 (1985).
- ¹⁸J. P. Perdew, K. Burke, M. Ernzerhof, "Generalized Gradient Approximation Made Simple", Phys. Rev. Lett. 77, 3865 (1996); Erratum: Phys. Rev. Lett. 78, 1396 (1997).
- ¹⁹S. Grimme, "Semiempirical GGA-type density functional constructed with a long-range dispersion correction", J. Comput. Chem. 27, 1787 (2006).
- ²⁰G. Levita, A. Cavaleiro, E. Molinari, T. Polcar, and M. C. Righi, "Sliding properties of MoS₂ layers: Load and interlayer orientation effects", J. Phys. Chem. C 118, 13809 (2014).

- ²¹G. Levita, E. Molinari, T. Polcar, M. C. Righi, "First-principles comparative study on the interlayer adhesion and shear strength of transition-metal dichalcogenides and graphene", Phys. Rev. B 92, 085434 (2015).
- ²²M. Ricci, A. Ambrosetti, P. L. Silvestrelli, "Improving the Description of Interlayer Bonding in TiS₂ by Density Functional Theory", J. Phys. Chem. C 124, 27592 (2020).
- ²³J. Zhou, S. Yang, Y. Zhang, J.-C. Ren, W. Liu, "Effective Descriptor for Screening Single-Molecule Conductance Switches", J. Am. Chem. Soc. 146, 6962 (2024); M. Fang, J. Han, S. He, J.-C. Ren, S. Li, W. Liu, "Effective Screening Descriptor for MXenes to Enhance Sulfur Reduction in Lithium–Sulfur Batteries", J. Am. Chem. Soc. 145, 12601 (2023); C. Chen, Y. Ma, K. Yao, Q. Ji, W. Liu, "Enantioselective adsorption on chiral ceramics with medium entropy", Nat. Commun. 15, 10105 (2024).
- ²⁴J. He, K. Hummer, and C. Franchini, "Stacking effects on the electronic and optical properties of bilayer transition metal dichalcogenides MoS₂, MoSe₂, WS₂ and WSe₂", Phys. Rev. B **89**, 075409 (2014).
- ²⁵W. O. Winer, "Molybdenum disulfide as a lubricant: A review of the fundamental knowledge", Wear 10, 422 (1967).
- ²⁶H.-P. Komsa and A. V. Krasheninnikov, "Effects of confinement and environment on the electronic structure and exciton binding energy of MoS₂ from first principles", Phys. Rev. B **86**, 241201(R) (2012).
- ²⁷M. Wolloch, G. Losi, M. Ferrario, M. C. Righi, "High-throughput screening of the static friction and ideal cleavage strength of solid interfaces", Sci. Rep. 9, 17062 (2019).
- ²⁸ M. Reguzzoni, A. Fasolino, E. Molinari, M. C. Righi, "Potential energy surface for graphene on graphene: Ab initio derivation, analytical description, and microscopic interpretation", Phys. Rev. B 86, 245434 (2012).
- ²⁹B. J. Irving, P. Nicolini, T. Polcar, "On the Lubricity of Transition Metal Dichalcogenides: An ab Initio Study", Nanoscale 9, 5597 (2017).

- ³⁰Y. Ma, Y. Dai, M. Guo, C. Niu, Y. Zhu, B. Huang, "Evidence of the Existence of Magnetism in Pristine VX₂ Monolayers (X = S, Se) and Their Strain-Induced Tunable Magnetic Properties", ACS Nano 6, 1695 (2012).
- ³¹M. Bonilla, S. Kolekar, Y. Ma, H. Coy Diaz, V. Kalappattil, R. Das, T. Eggers, H. R. Gutierrez, M.-H. Phan, M. Batzill, "Strong room-temperature ferromagnetism in VSe₂ monolayers on van der Waals substrates", Nature Nanotechnology 13, 289 (2018).
- ³²A. Samad, Y.-H. Shin, "MoS₂@VS₂ Nanocomposite as a Superior Hybrid Anode Material", ACS Appl. Mater. Interfaces 9, 29942 (2017).
- ³³L. Li, Z. Li, A. Yoshimura, C. Sun, T. Wang, Y. Chen, Z. Chen, A. Littlejohn, Y. Xiang, P. Hundekar, S. F. Bartolucci, J. Shi, S.-F. Shi, V. Meunier, G.-C. Wang, N. Koratkar, "Vanadium disulfide flakes with nanolayered titanium disulfide coating as cathode materials in lithium-ion batteries", Nature Communications 10, 1764 (2019).
- ³⁴M. Esters, R. G. Hennig, D. C. Johnson, "Dynamic instabilities in strongly correlated VSe₂ monolayers and bilayers", Phys. Rev. B 96, 235147 (2017).
- ³⁵S. Grimme, J. Antony, S. Ehrlich, H. Krieg, "A consistent and accurate ab initio parametrization of density functional dispersion correction (DFT-D) for the 94 elements H-Pu", J. Chem. Phys. **132**, 154104 (2010).
- ³⁶R. Sabatini, T. Gorni, S. de Gironcoli, "Nonlocal van der Waals density functional made simple and efficient", Phys. Rev. B 87, 041108 (2013).
- ³⁷O. A. Vydrov, T. Van Voorhis, "Nonlocal van der Waals density functional: The simpler the better", J. Chem. Phys. **133**, 244103 (2010).
- ³⁸T. Björkman, A. Gulans, A. V. Krasheninnikov, R. M. Nieminen, "van der Waals Bonding in Layered Compounds from Advanced Density-Functional First-Principles Calculations", Phys. Rev. Lett. **108**, 235502 (2012).
- ³⁹M. Wolloch, G. Levita, P. Restuccia, M. C. Righi, "Interfacial Charge Density and Its Connection to Adhesion and Frictional Forces", Phys. Rev. Lett. 121, 026804 (2018).
- ⁴⁰M. R. Vazirisereshk, K. Hasz, M.-Q. Zhao, A. T. C. Johnson, R. W. Carpick, A. Martini, "Nanoscale Friction Behavior of Transition-Metal Dichalcogenides: Role of the Chalcogenide", ACS Nano 14, 16013 (2020).